Inorg. Chem. **2006**, *45*, 6152–6160

Series of New Cationic Iridium(III) Complexes with Tunable Emission Wavelength and Excited State Properties: Structures, Theoretical Calculations, and Photophysical and Electrochemical Properties

Qiang Zhao, Shujuan Liu, Mei Shi, Chuanming Wang, Mengxiao Yu, Lei Li, Fuyou Li,* Tao Yi, and Chunhui Huang*

Department of Chemistry & Laboratory of Advanced Materials, Fudan University, Shanghai, 200433, P. R. China

Received November 27, 2005

A series of new cationic iridium(III) complexes $[Ir(piq)_2(N\wedge N)]^+PF_6^-$ (**1**–**6**) (piq =1-phenyl-isoquinoline) containing N∧N ligands with different conjugated lengths were synthesized, where the six N∧N ligands were bipyridine, phenanthroline, 2-pyridyl-quinoline, 2,2′-biquinoline, 1,1′-biisoquinoline, and 2-(2-quniolinyl)quinoxaline. Single-crystal X-ray diffraction spectra of three complexes were studied, and the iridium(III) centers were found to adopt a distorted octahedral coordination geometry with cis metalated carbons and trans nitrogen atoms. UV–vis, photoluminescence, cyclic voltammetry, and theoretical calculations were employed for studying the photophysical and electrochemical properties. And the excited-state properties were investigated in detail. The excited state of complexes is complicated and contains triplet metal-to-ligand charge transfer (^{3}MLCT), triplet ligand-to-ligand charge transfer (^{3}LLCT), and ligand-centered (cyclometalated) (^{3}LC) transitions simultaneously. Importantly, the emission wavelength can be tuned significantly from 586 to 732 nm by changing the conjugated length of N∧N ligands.

Introduction

Recently, heavy-metal complexes, particularly iridium(III) complexes have received considerable attention because of their high phosphorescence quantum efficiencies and applications in organic light-emitting devices (OLEDs)[1] and luminescent biological-labeling reagents.[2] The high emission efficiency is caused by spin−orbit coupling which leads to the mixed singlet and triplet metal-to-ligand charge-transfer states and creates the possibility of full utilization of both the singlet and triplet excitons.

The iridium(III) complexes can be divided into two classes. The first is the neutral complexes containing cyclometalated ligands and other anionic ligands.[3] This class of iridium(III) complexes has received extensive study because of their high quantum yields and application in highly efficient organic electroluminescence devices.[1] The emission wavelength and excited-state lifetime can be tuned by changing cyclometalated ligands.

The other class of complexes is cationic iridium(III) complexes containing bidentate ligands (e.g., bipyridine and phenanthroline derivatives). The synthesis of cationic complexes can be carried out under mild conditions. Because of their rich photophysical properties, ionic character, and good solubility in polar solvents and even in aqueous media,

* To whom correspondence should be addressed. Fax: 86-21-55664621. Phone: 86-21-55664185. E-mail: fyli@fudan.edu.cn (F.Y.L.); chhuang@pku.edu.cn (C.H.H.).

(1) (a) Lamansky, S.; Djurovich, P.; Murphy, D.; Abdel-Razzaq, F.; Lee, H. E.; Adachi, C.; Burrows, P. E.; Forrest, S. R.; Thompson, M. E. *J. Am. Chem. Soc.* **2001**, *123*, 4304−4312. (b) Zhu, W.; Mo, Y.; Yuan, M.; Yang, W.; Cao, Y. *Appl. Phys. Lett.* **2002**, *80*, 2045−2047. (c) Gong, X.; Ostrowski, J. C.; Bazan, G. C.; Moses, D.; Heeger, A. J. *Appl. Phys. Lett.* **2002**, *81*, 3711−3713. (d) Thomas, K. R. J.; Velusamy, M.; Lin, J. T.; Chien, C. H.; Tao, Y. T.; Wen, Y. S.; Hu, Y. H.; Chou, P. T. *Inorg. Chem.* **2005,** *44*, 5677−5685. (e) Chan, S. C.; Chan, M. C. W.; Wang, Y.; Che, C. M.; Cheung, K. K.; Zhu, N. *Chem.—Eur. J.* **2001**, *7*, 4180−4190. (f) Lu, W.; Mi, B. X.; Chan, M. C. W.; Hui, Z.; Che, C. M.; Zhu, N.; Lee, S. T. *J. Am. Chem. Soc.* **2004**, *126*, 4958−4971. (g) Huang, C. H.; Li, F. Y.; Huang, W. *Introduction to Organic Light-Emitting Materials and Devices*; Press of Fudan University: Shanghai, 2005.

(2) (a) Lo, K. K. W.; Ng, D. C. M.; Chung, C. K. *Organometallics* **2001**, *20*, 4999−5001. (b) Lo, K. K. W.; Chan, J. S. W.; Lui, L. H.; Chung, C. K. *Organometallics* **2004**, *23*, 3108−3116. (c) Lo, K. K. W.; Chung, C. K.; Lee, T. K. M.; Lui, L. H.; Tsang, K. H. K.; Zhu, N. *Inorg. Chem.* **2003**, *42*, 6886−6897. (d) Lo, K. K. W.; Li, C. K.; Lau, J. S. Y. *Organometallics* **2005**, *24*, 4594−4601.

(3) (a) Coppo, P.; Plummer, E. A.; De Cola, L. *Chem. Commun.* **2004**, 1774−1775. (b) Lamansky, S.; Djurovich, P.; Murphy, D.; Abdel-Razzaq, F.; Kwong, R.; Tsyba, I.; Bortz, M.; Mui, B.; Bau, R.; Thompson, M. E. *Inorg. Chem.* **2001**, 40, 1704−1711. (c) Wilkinson, A. J.; Goeta, A. E.; Foster, C. E.; Williams, J. A. G. *Inorg. Chem.* **2004**, 43, 6513−6515.

10.1021/ic052034j CCC: $33.50
Published on Web 07/11/2006

Scheme 1 Chemical Structures of the Iridium Complexes **1**−**6**

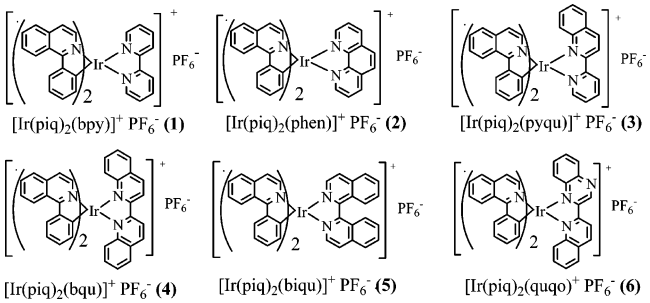

cationic iridium(III) complexes have also attracted many attentions.[4] Applications of cationic iridium(III) complexes as biological-labeling reagents and chemosensors for oxygen,[5] protons,[6] chloride ions[7] have been described recently. There have been some reports about the cationic iridium(III) complexes containing different bipyridine derivatives.[8] Most of these reports are focused on the effect on the photophysical properties of different substituents of bipyridine ligands. Changing the substituents of bipyridine ligands can tune the photophysical properties, especially the emission wavelength. However, the tuning of emission wavelength by changing the substituents is not very evident.[8b] In this paper, we synthesized a series of new cationic 1-phenylisoquinoline-based (piq-based) iridium(III) complexes $[Ir(piq)_2(N\wedge N)]^+PF_6^-$ **(1**−**6)** containing N∧N ligands with different conjugated lengths. Herein, the six N∧N ligands were bipyridine (bpy), phenanthroline (phen), 2-pyridinylquinoline (pyqu), 2,2′-biquinoline (bqu), 1,1′-biisoquinoline (biqu) and 2-(2-quniolinyl)quinoxaline (quqo), respectively. The chemical structures of these cationic iridium(III) complexes are shown in Scheme 1. Compared with the change of substituents of bipyridine ligands, the variation of conjugated length of N∧N ligands can significantly influence the photophysical properties, especially the emission wavelength, and the emission wavelengths of these complexes can be tuned within a wide range, from 586 to 732 nm. Moreover, the excited-state properties of these complexes were investigated by theoretical calculations and photophysical and electrochemical properties.

Experimental Section

Materials. All reagents and chemicals were procured from commercial sources and used without further purification. Bipyridine (bpy), phenanthroline (phen), 2-acetylpyridine 1-bromoisoquinoline, and 2-aminobenzadehyde were obtained from Acros. 2-Acetylquinoxaline was synthesized according to previous report.[9]

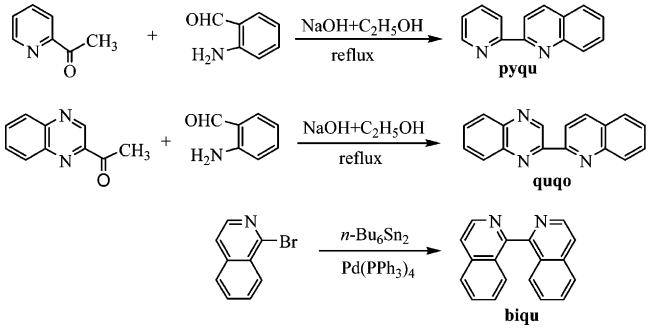

Figure 1. Synthetic routines of the ligands pyqu, quqo, and biqu.

General Experiments. ^{1}H NMR spectra were recorded with a Varian spectrometer at 400 MHz. Mass spectra were obtained on SHIMADZU matrix-assisted laser desorption/ionization time-of-flight mass spectrometer (MALDI-TOF-MASS). Elemental analyses were carried out with a VarioEL III O-Element Analyzer system. The UV−vis spectra were recorded on a Shimadzu UV-2550 spectrometer. Steady-state emission experiments at room temperature were measured on an Edinburgh LFS-920 spectrometer. Lifetime studies were performed with an Edinburgh LFS-920 spectrometer with a hydrogen-filled excitation source. The data were analyzed by iterative convolution of the luminescence decay profile with the instrument response function using a software package provided by Edinburgh Instruments. The luminescence quantum yields of complexes in solution were measured with reference to quinine sulfate ($\Phi_F = 0.564$ in 1 mol L^{-1} sulfuric acid). The solution was degassed by three freeze−pump−thaw cycles.

Synthesis of the Ligands. 2-Pyridinyl-quinoline (pyqu). The ligands pyqu and quqo were synthesized according to Friedländer condensation[10] (see Figure 1). Herein, a detailed description was provided only for pyqu. Saturated ethanolic NaOH was added to a mixture of 2-acetylpyridine (500 mg, 4.13 mmol) and 2-aminobenzadehyde (500 mg, 4.13 mmol) in ethanol, and the mixture was refluxed overnight. After the mixture was cooled, the precipitate was collected by filtration and recrystallized from a CH_2Cl_2 solution to obtain white crystals (595 mg) in 70% yield. NMR (400 MHz, $CDCl_3$): δ 8.74 (d, 1H), 8.65 (d, 1H), 8.56 (d, 1H), 8.29 (d, 1H), 8.18 (d, 1H), 7.83−7.91 (m, 2H), 7.74 (t, 1H), 7.55 (t, 1H), 7.36 (t, 1H). Anal. Calcd for $C_{14}H_{10}N_2$: C, 81.53; H, 4.89; N, 13.58. Found: C, 81.92; H, 5.37; N, 13.26.

2-(2-Quniolinyl)quinoxaline (quqo). White crystals. Yield: 65%. NMR (400 MHz, $CDCl_3$): δ 10.23 (s, 1H), 8.77 (d, 1H), 8.37 (d, 1H), 8.28 (d, 1H), 8.18−8.22 (m, 2H), 7.90 (d, 1H), 7.77−7.83 (m, 3H), 7.62 (t, 1H). Anal. Calcd for $C_{17}H_{11}N_3$: C, 79.36; H, 4.31; N, 16.33. Found: C, 79.11; H, 4.47, N, 16.55.

1,1′-Biisoquinoline (biqu). Biqu was prepared by a similar method which was reported previously.[11] White crystals. Yield: 30%. NMR (400 MHz, $CDCl_3$): δ 8.42 (d, 1H), 7.64−7.69 (m, 4H), 7.51−7.57 (m, 3H), 7.45−7.48 (m, 3H), 6.55 (d,1H). Anal. Calcd for $C_{18}H_{12}N_2$: C, 84.35; H, 4.72; N, 10.93. Found: C, 83.92; H, 4.47; N, 11.25.

(4) (a) Garces, F. O.; King, K. A.; Watts, R. J. *Inorg. Chem.* **1988**, *27*, 3464−3471. (b) Colombo, M. G.; Hauser, A.; Güdel, H. U. *Inorg. Chem.* **1999**, *38*, 2250−2258. (c) Neve, F.; Crispini, A.; Serroni, S.; Loiseau, F.; Campagna, S. *Inorg. Chem.* **2001**, 40, 1093−1101. (d) Yutaka, T.; Obara, S.; Ogawa, S.; Nozaki, K.; Ikeda, N.; Ohno, T.; Ishii, Y.; Sakai, K.; Haga, M. *Inorg. Chem.* **2005**, *44*, 4737−4746.
(5) Di Marco, G.; Lanza, M.; Mamo, A.; Stefio, I.; Di Pietro, C.; Romeo, G.; Campagna, S. *Anal. Chem.* **1998**, *70*, 5019−5023.
(6) Licini, M.; Williams, J. A. G. *Chem. Commun.* **1999**, 1943−1944.
(7) Goodall, W.; Williams, J. A. G. *J. Chem. Soc., Dalton Trans*. **2000**, 2893−2896.
(8) (a) Neve, F.; Deda, M. L.; Crispini, A.; Bellusci, A.; Puntoriero, F.; Campagna, S. *Organometallics* **2004**, *23*, 5856−5863. (b) Lepeltier, M.; Lee, T. K. M.; Lo, K. K. W.; Toupet, L.; Bozec, H. L.; Guerchais, V. *Eur. J. Inorg. Chem.* **2005**, 110−117.
(9) Rowe, D. J.; Garner, D. C.; Joule, J. A. *J. Chem. Soc., Perkin. Trans. 1*. **1985**, 1907−1910.
(10) Hu, Y. Z.; Zhang, G.; Thummel, R. P. *Org. Lett.* **2003**, *5*, 2251−2253.
(11) Schwab, P. F. H.; Fleischer, F.; Michl, J. *J. Org. Chem.* **2002**, *67*, 443−449.

1-Phenyl-isoquinoline (piq). Piq was synthesized according to the previous report.[12] White solid. Yield: 84%. NMR (400 MHz, $CDCl_3$): δ 8.61 (d, 1H), 8.10 (d, 1H), 7.87 (d, 1H), 7.63−7.72 (m, 4H), 7.49−7.56 (m, 4H). Anal. Calcd for $C_{15}H_{11}N$: C, 87.77; H, 5.40; N, 6.82. Found: C, 87.72; H, 5.30; N, 6.69.

Synthesis of the Iridium(III) Complexes. All iridium(III) complexes $[Ir(piq)_2L]^+PF_6^-$ were prepared by the same procedure. Herein, only the synthesis of $[Ir(piq)_2(bpy)]^+PF_6^-$ is described in detail.

$[Ir(piq)_2(bpy)]^+PF_6^-$ (1). The cyclometalated iridium(III) chloro-bridged dimer $[Ir(piq)_2Cl]_2$ was prepared according to literature methods.[13] The solution of $[Ir(piq)_2Cl]_2$ (0.10 g, 0.079 mmol) and bpy (0.024 g, 0.158 mmol) in CH_2Cl_2−MeOH (30 mL, 2:1 v/v) was heated to reflux. After 4 h, the red solution was cooled to room temperature, and then a 10-fold excess of potassium hexafluorophosphate was added. The suspension was stirred for 2 h, and then it was filtered to remove insoluble inorganic salts. The solution was evaporated to dryness under reduced pressure. It was chromatographed with CH_2Cl_2/ acetone (15:1) to produce a red solid in a 65% yield. ^{1}H NMR (400 MHz, $CDCl_3$): δ 8.93 (m, 2H), 8.72 (d, 2H), 8.28 (d, 2H), 8.15 (t, 2H), 7.89−7.92 (m, 2H), 7.74−7.79 (m, 6H), 7.35−7.39 (m, 5H), 7.10−7.14 (t, 2H), 6.90 (t, 2H), 6.30 (d, 2H), 5.30 (s, 1H). Anal. Calcd for $IrC_{40}H_{28}N_4F_6P$: C, 53.27; H, 3.13; N, 6.21. Found: C, 53.01; H, 3.57; N, 6.46. MS (MALDI-TOF): *m*/*e* 755.0 (M − PF_6).

$[Ir(piq)_2(phen)]^+PF_6^-$ (2). Yield: 70%. ^{1}H NMR (400 MHz, $CDCl_3$): δ 8.95 (d, 2H), 8.69 (d, 2H), 8.31 (d, 2H), 8.29 (s, 2H), 8.07 (d, 2H), 7.85 (d, 2H), 7.70−7.83 (m, 6H), 7.14−7.26 (m, 6H), 6.75 (t, 2H), 6.40 (d, 2H). Anal. Calcd for $IrC_{42}H_{28}N_4F_6P$: C, 54.48; H, 3.05; N, 6.05. Found: C, 54.65; H, 3.42; N, 6.33. MS (MALDI-TOF): *m*/*e* 780.2 (M − PF_6).

$[Ir(piq)_2(pyqu)]^+PF_6^-$ (3). Yield: 61%. ^{1}H NMR (400 MHz, $CDCl_3$): δ 8.98 (d, 1H), 8.91 (d, 1H), 8.79 (m, 2H), 8.61 (d, 1H), 8.31 (d, 1H), 8.22 (m, 2H), 8.04 (d, 1H), 7.79−7.90 (m, 5H), 7.63−7.69 (m, 3H), 7.47 (t, 1H), 7.37 (t, 1H), 7.26−7.30 (m, 4H), 7.09−7.17 (m, 3H), 6.86−6.94 (m, 2H), 6.37 (d, 1H), 6.20 (d, 1H). Anal. Calcd for $IrC_{44}H_{30}N_4F_6P$: C, 55.52; H, 3.18; N, 5.89. Found: C, 55.31; H, 3.45; N, 5.64. MS (MALDI-TOF): *m*/*e* 805.5 (M − PF_6).

$[Ir(piq)_2(bqu)]^+PF_6^-$ (4). Yield: 53%. ^{1}H NMR (400 MHz, $CDCl_3$): δ 8.77 (d, 4H), 8.62 (d, 2H), 8.18 (d, 2H), 7.85 (d, 4H), 7.70−7.77 (m, 6H), 7.63 (d, 2H), 7.45 (t, 2H), 7.24 (d, 2H), 7.06−7.11 (m, 4H), 6.86 (t, 2H), 6.44 (d, 2H). Anal. Calcd for $IrC_{48}H_{32}N_4F_6P$: C, 57.54; H, 3.22; N, 5.59. Found: C, 57.01; H, 3.53; N, 5.19. MS (MALDI-TOF): *m*/*e* 855 (M − PF_6).

$[Ir(piq)_2(biqu)]^+PF_6^-$ (5). Yield: 45%. ^{1}H NMR (400 MHz, $CDCl_3$): δ 8.91 (d, 2H), 8.25 (d, 2H), 8.04 (t, 5H), 7.92 (d, 2H), 7.82 (t, 5H), 7.71−7.76 (m, 8H), 7.64 (t, 2H), 7.12 (t, 2H), 6.92 (t, 2H), 6.70 (d, 2H). Anal. Calcd for $IrC_{48}H_{32}N_4F_6P$: C, 57.54; H, 3.22; N, 5.59. Found: C, 57.78; H, 3.47; N, 5.23. MS (MALDI-TOF): *m*/*e* 855.3 (M − PF_6).

$[Ir(piq)_2(quqo)]^+PF_6^-$ (6). Yield: 50%. ^{1}H NMR (400 MHz, $CDCl_3$): δ 10.04 (s, 1H), 8.82−8.89 (m, 2H), 8.70−8.76 (m, 2H), 8.25 (d, 1H), 8.17 (t, 2H), 7.831−7.90 (m, 3H), 7.63−7.78 (m, 8H), 7.58 (d, 1H), 7.49 (t, 1H), 7.29 (d, 2H), 7.20 (t, 1H), 7.09−7.16 (m, 3H), 6.97−6.92 (m, 2H), 6.34−6.41 (m, 2H). Anal. Calcd for $IrC_{47}H_{31}N_5F_6P$: C, 56.28; H, 3.11; N, 6.98. Found: C, 56.53; H, 3.32; N, 6.45. MS (MALDI-TOF): *m*/*e* 856.2 (M − PF_6).

Theoretical Calculations. The optimization of the complex structures was performed using B3LYP density functional theory. The LANL2DZ basis set was used to treat the Ir atom, whereas the 3-21G* basis set was used to treat all other atoms. The contours of the HOMO and LUMO orbitals were plotted.

Scheme 2. Chemical Structure of $[Ir(piq)_2(phen)]^+ClO_4^-$ (**2′**)

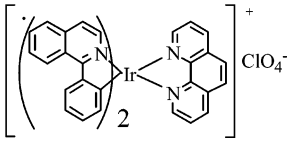

Electrochemical Measurements. Electrochemical measurements were performed with an Eco Chemie Autolab. All measurements were carried out in a one-compartment cell under N_2 gas, equipped with a glassy-carbon working electrode, a platinum wire counter electrode, and a Ag/Ag^+ reference electrode. The supporting electrolyte was a 0.10 mol L^{-1} acetonitrile solution of tetrabutylammonium hexafluorophosphate (Bu_4NPF_6).

X-ray Crystallography Analysis. The single crystals of complexes **5**, **6**, and $[Ir(piq)_2(phen)]^+ClO_4^-$ (**2′**) (see Scheme 2) were mounted on glass fiber and transferred to a Bruker SMART CCD area detector. Crystallographic measurement was carried out using a Bruker SMART CCD diffractometer, σ scans, and graphite-monochromated Mo Kα radiation (λ = 0.71073 Å) at room temperature. The structure was solved by direct methods and refined by full-matrix least-squares on F^2 using the program SHELXS-97.[14] All non-hydrogen atoms were refined anisotropically. Hydrogen atoms were calculated in ideal geometries. For the full-matrix least-squares refinements [$I > 2\sigma(I)$], the unweighted and weighted agreement factors of $R1 = \sum(F_o - F_c)/\sum F_o$ and $wR2 = [\sum w(F_o^2 - F_c^2)^2/\sum wF_o^4]^{1/2}$ were used. CCDC reference numbers for **2′**, **5**, and **6** are 288649, 288650 and 288651, respectively.

Results and Discussion

Synthesis. The Friedländer condensation[10] is a convenient way to synthesize quinoline derivatives because of its high yield, low cost, short reaction time, and facile manipulation. In this work, the N∧N ligands pyqu and quqo were synthesized by the Friedländer condensation (see Figure 1) with high yields of 70 and 65%, respectively. The synthesis of biqu was carried out according to the similar methods reported previously.[11] However, the yields of reaction was low in our work, about 30%.

The synthetic procedure for the cationic iridium(III) complexes, $[Ir(piq)_2L]^+PF_6^-$, has two steps. The dinuclear cyclometalated iridium(III) chloro-bridged precursor, $[Ir(piq)_2Cl]_2$, was synthesized by the same methods reported by Nonoyama.[13] Then the cationic iridium(III) complexes were synthesized by the bridge-splitting reactions of $[Ir(piq)_2Cl]_2$ and, consequently, complexing with the corresponding diimine ligands (L = bpy, phen, pyqu, bqu, biqu and quqo). Compared with the synthesis of neutral iridium(III) complexes containing β-diketone ligands which needs a harsh reaction condition (reflux in a high-boiling solvent mixture) and a much longer reaction time, the synthesis of cationic iridium complexes $[Ir(piq)_2L]^+PF_6^-$ can be carried out under mild reaction conditions. In our case, new iridium(III) complexes with lesser decomposition,

(12) Tsuboyama, A.; Iwawaki, H.; Furugori, M.; Mukaide, T.; Kamatani, J.; Igawa, S.; Moriyama, T.; Miura, S.; Takiguchi, T.; Okada, S.; Hoshino, M.; Ueno, K. *J. Am. Chem. Soc.* **2003**, *125*, 12971−12979.
(13) Nonoyama, K. *Bull. Chem. Soc. Jpn.* **1974**, *47*, 467−468.
(14) Sheldrick, G. M. *SHELXTL-Plus V5.1 Software Reference Manual*; Bruker AXS Inc.: Madison, WI, 1997.

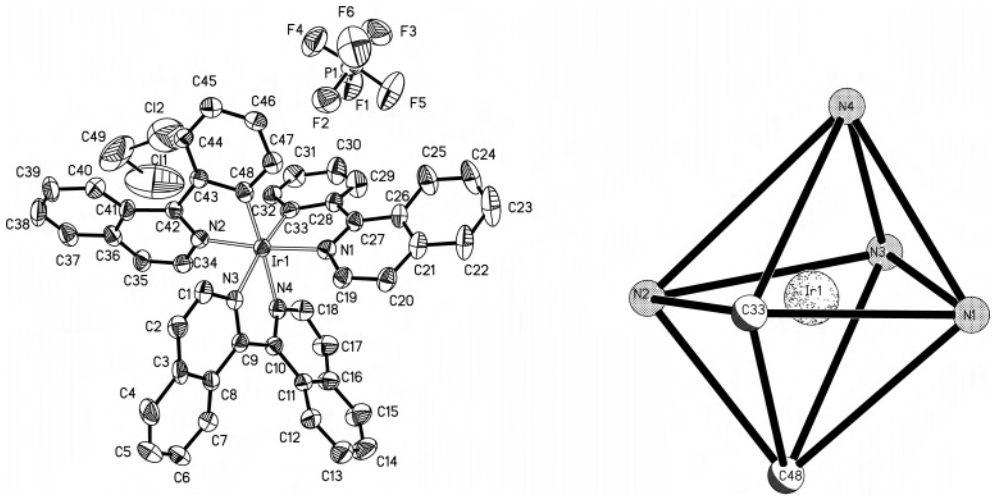

Figure 2. ORTEP diagram of $[Ir(piq)_2(biqu)]^+PF_6^-$ (**5**) and its coordination polyhedron.

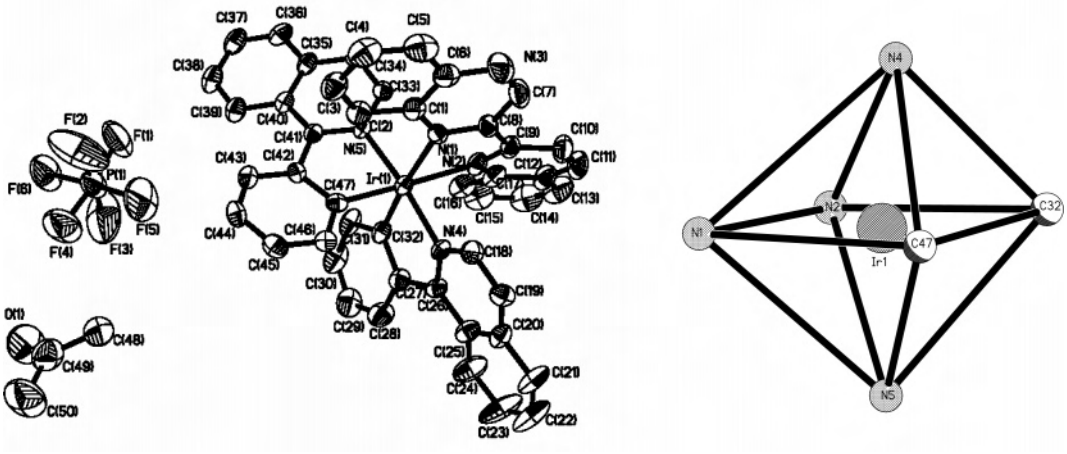

Figure 3. ORTEP diagram of $[Ir(piq)_2(quqo)]^+PF_6^-$ (**6**) and its coordination polyhedron.

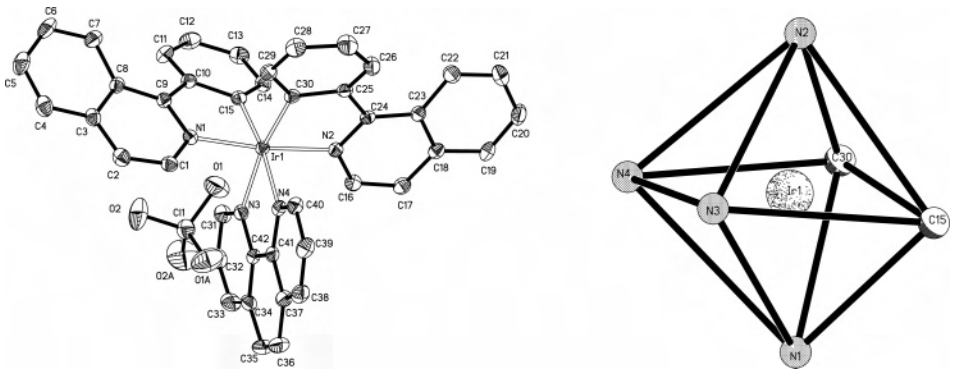

Figure 4. ORTEP diagram of $[Ir(piq)_2(phen)]^+ClO_4^-$ (**2′**) and its coordination polyhedron.

limited workup, and good yields were obtained.[15] These complexes were characterized successfully through ^1H NMR, MALDI-TOF, and elemental analysis.

Crystal Structures of 5, 6 and 2′. The single crystals of **5** and **6** were obtained from the mixed solution of CH_2Cl_2 and hexane. Interestingly, when the CH_3CN solution of $[Ir(piq)_2(phen)]^+ PF_6^-$ (**2**) containing tetrabutylammonium perchlorate was evaporated slowly, we obtained a new iridium complex $[Ir(piq)_2(phen)]^+ ClO_4^-$ with ClO_4^- instead of PF_6^- as the anion, which was named as **2′** (see Scheme 2). This fact indicates that the PF_6^- anion of **2** is easily exchanged with the ClO_4^- anion. Figures 2−4 show the ORTEP views and coordination polyhedrons of **5**, **6**, and **2′**, respectively. The crystallographic refinement parameters of **5**, **6**, and **2′** are summarized in Table 1. Selected relevant bond parameters are listed in Table 2.

(15) (a) Nazeeruddin, Md. K.; Humphry-Baker, R.; Berner, D.; Rivier, S.; Zuppiroli, L.; Graetzel, M. *J. Am. Chem. Soc.* **2003**, *125*, 8790−8797. (b) Neve, F.; Crispini, A.; Loiseau, F.; Campagna, S. *Dalton Trans.* **2000**, 1399−1401. (c) Neve, F.; Crispini, A.; Serroni, S.; Loiseau, F.; Campagna, S. *Inorg. Chem.* **2001**, *40*, 1093−1101. (d) Lo, K. K.-W.; Chung, C. K.; Zhu, N. *Organometallics* **2003**, *22*, 475−479. (e) Plummer, E. A.; Hofstraat, J. W.; De Cola, L. *Dalton Trans.* **2003**, 2080−2084.

Table 1. Crystallographic Data for **5**, **6** and **2′**

	5·CH_2Cl_2	**6**·acetone	**2′**
emipirical formula	$C_{49}H_{34}Cl_2F_6IrN_4P$	$C_{50}H_{37}F_6IrN_5OP$	$C_{42}H_{28}ClIr_4O_4$
cryst syst	triclinic	monoclinic	monoclinic
space group	$P\bar{1}$	$P2_1/c$	$C2/c$
cryst size (mm)	0.30 × 0.30 × 0.20	0.25 × 0.20 × 0.08	0.06 × 0.05 × 0.04
a (Å)	11.919(2)	9.7137(19)	31.645(6)
b (Å)	14.675(3)	30.905(6)	10.500(2)
c (Å)	15.736(3)	14.557(3)	20.926(4)
α (deg)	116.18(3)	90	90
β (deg)	94.94(3)	100.753(2)	106.64(3)
γ (deg)	98.50(3)	90	90
V (Å^3)	2407.1(8)	4293.1(14)	6662(2)
Z	2	4	8
calcd density (g cm^{-3})	1.500	1.642	1.755
μ (mm^{-1})	2.978	3.219	4.141
F(000)	1072	2104	3472
final R1 [$I > 2\sigma(I)$]	0.0573	0.0508	0.0264
wR2 [$I > 2\sigma(I)$]	0.1389	0.1169	0.0710
R1 (all data)	0.0885	0.0753	0.0319
wR2 (all data)	0.1560	0.1322	0.0742
GOF on F^2	0.977	1.092	1.056

From Figures 2−4, we can see that the iridium(III) centers in the three complexes adopt a distorted octahedral coordination geometry with cis metalated carbons and trans nitrogen atoms, as revealed by previous structural studies on mononuclear species containing the C∧N cyclometalated ligands.[8a] Moreover, it can be seen from Table 2 that the distances of Ir−C (∼2.00 Å) and Ir−N (C∧N) (∼2.04 Å) are the same in all three complexes. The Ir−N (N∧N ligands) distances, however, are longer than the distances of Ir−N (C∧N ligands) for the three complexes. For example, the Ir−N (biqu) distances (2.142(7) and 2.161(7) Å) are longer than the corresponding Ir−N (piq) distances (2.028(7) and 2.037(7) Å) in **5** because of their trans influence. Similar phenomena are also observed for **2′** and **6**. In addition, the Ir−N (quqo) distances in **6** are longer than those in **2′** and **5**. We propose that the elongated Ir−N (N∧N ligand) bonds in **6** are the result of the weaker basicity of quinoxaline in comparison with that of quinoline and pyridine. It can be seen from Table 2 that the bite angles for the diimine ligand, phen, biqu, and quqo, chelates are 77.8, 74.7, and 74.8°, respectively. The relatively wider bite angle of (N−Ir−N) in **2′** may be caused by the planar structure of phen. Similar to other related complexes,[8a] the $[Ir(piq)_2(biqu)]^+$ and $[Ir(piq)_2(quqo)]^+$ cations are connected to the PF_6^- anion by weak intra- and intermolecular C−H···F−P hydrogen bonds with an average H···F diatance of 2.60 Å.

The comparison of the structural parameters observed for these complexes with the previously known related complexes is noteworthy. The selected bond lengths and angles for a few recently reported iridium(III) complexes $[Ir(ppy)_2(di\text{-}C_9H_{19}\text{-}bpy)]^+PF_6^-$ (ppy = 2-phenylpyridine) [8a] and $Ir(piq)_3$[12] are also listed in Table 2. Compared with the $[Ir(ppy)_2]^+$ cation [8a] and $Ir(piq)_3$,[12] reported previously in the other systems, $[Ir(piq)_2]^+$ in complexes **5**, **6**, and **2′** shows shorter bond distances of Ir−C. This fact indicates a stronger σ donation from the 1-phenylisoquinoline ligand in **5**, **6**, and **2′**.

Absorption Spectroscopy. The UV−vis absorption spectra of the complexes are shown in Figure 5, and the electronic absorption data are listed in Table 3. All complexes display intense absorption bands below 400 nm, moderately intense absorption bands in the range 400−500 nm, and weak absorption bands above 500 nm. The absorption bands at λ < 400 nm are similar to those of the corresponding free piq and diimine ligands and are assigned to spin-allowed intraligand LC($\pi \rightarrow \pi^*$) (diimine and piq) transitions. According to the previous study,[8a] both ligand-to-ligand charge transfer (LLCT)[8a] and metal-to-ligand charge transfer (MLCT)[16] may contribute to the visible-region charge transfer (CT) bands. Therefore, we believe that the moderately intense absorptions at ca. 400−500 nm and weaker absorptions above 500 nm may receive contributions from LLCT, ^{1}MLCT, and ^{3}MLCT for complexes **1**−**6**.

Table 2. Coordination Bonding Parameters (Å, deg) Observed in the Iridium(III) Complexes

complexes	Ir−C	Ir−$N_{(CN)}$	Ir−$N_{(NN)}$	C−Ir−C	C−Ir−$N_{(CN)}$	C−Ir−$N_{(NN)}$	$N_{(CN)}$−Ir−$N_{(CN)}$	$N_{(CN)}$−Ir−$N_{(NN)}$	$N_{(NN)}$−Ir−$N_{(NN)}$
$[Ir(piq)_2(biqu)]^+PF_6^-$ (**5**)	1.984(9)	2.028(7)	2.142(7)	89.5(3)	96.7(3)	170.7(3)	174.0(3)	85.9(3)	74.7(3)
	2.002(9)	2.037(7)	2.161(7)		79.3(3)	99.7(3)		97.9(3)	
					80.2(3)	96.1(3)		100.4(3)	
					95.5(3)	174.4(3)		85.0(3)	
$[Ir(piq)_2(quqo)]^+PF_6^-$ (**6**)	1.987(7)	2.032(5)	2.213(6)	81.7(3)	79.5(2)	177.0(2)	173.4(2)	100.6(2)	74.8(2)
	2.014(8)	2.056(5)	2.214(6)		95.4(3)	101.3(3)		83.6(2)	
					96.6(2)	102.1(2)		89.6(2)	
					78.8(3)	174.3(2)		96.4(2)	
$[Ir(piq)_2(phen)]^+ClO_4^-$ (**2′**)	1.997(4)	2.047(3)	2.146(3)	93.89(14)	94.82(13)	169.37(13)	173.08(11)	91.96(11)	77.76(11)
	2.001(4)	2.053(3)	2.148(3)		79.76(12)	95.37(12)		94.06(11)	
					79.71(13)	93.38(13)		95.88(11)	
					96.28(13)	171.81(12)		88.72(11)	
$[Ir(ppy)_2(di\text{-}C_9H_{19}\text{-}bpy)]^+PF_6^-$ [8a]	2.015(7)	2.057(6)	2.151(6)	94.5(4)	80.1(3)	170.3(3)	172.7(4)	89.9(2)	76.3(3)
					94.9(3)			95.9(2)	
$Ir(piq)_3$[12]	2.009(6)	2.135(5)		119.7(5)	78.5(2)				

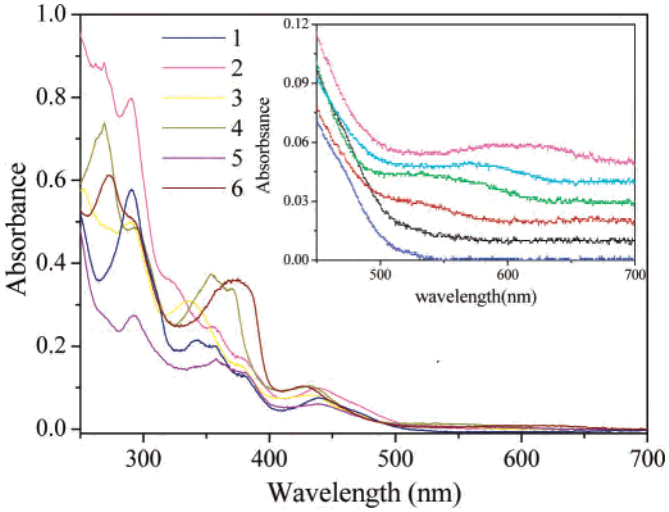

Figure 5. Absorption spectra of **1**−**6** in CH_2Cl_2.

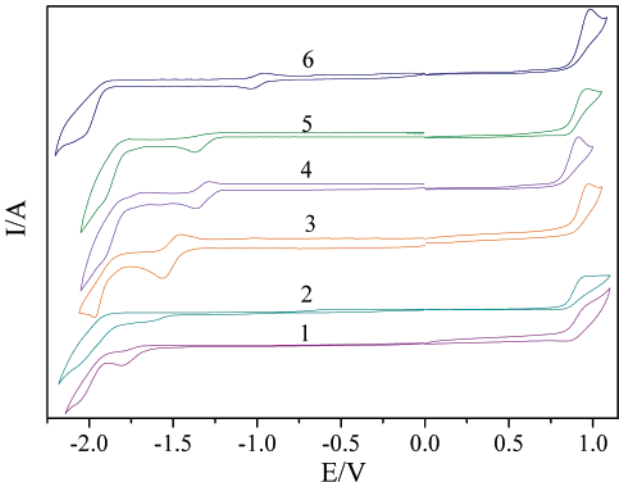

Figure 6. Cyclic voltammograms of **1**−**6** (scan rate = 50 mV s^{-1}).

Table 3. Absorption Data of **1**−**6** in CH_2Cl_2 at 298 K

	λ_{abs}(log ϵ) [nm]
1	290(5.76), 344(5.33), 355(5.30), 378(5.11), 439(4.88), 506(3.33)
2	269(5.95), 290(5.90), 353(5.39), 437(5.00), 506(4.18)
3	289(5.70), 336(5.49), 379(5.18), 432(4.92), 536(3.95)
4	269(5.87), 292(5.69), 354(5.57), 370(5.53), 431(5.02), 551(4.11) sh
5	292(5.44), 357(5.23), 380(5.14), 440(4.79), 570(3.78) sh
6	273(5.79), 375(5.56), 425(5.02), 602(3.95) sh

Electrochemical Properties. The electrochemical properties of the complexes were studied by cyclic voltammetry (see Figure 6). The HOMO and LUMO energy can be deduced by the equation $E_{HOMO(LUMO)} = -(4.80 + E_{onset})$.[1d] The data are listed in Table 4. All complexes exhibit an irreversible oxidation wave at similar potential between 0.92 and 0.98 V. It is assumed that the pure metal-centered oxidation is reversible and that the irreversibility increases as the contribution to HOMO of the cyclometalating phenyl(s) increases.[16e,17] Therefore, the irreversible oxidation processes of **1**−**6** could be assigned to orbits receiving a strong contribution from iridium center and Ir−C^- σ-bond orbits simultaneously. The oxidation processes of all complexes at different scan rates of 20, 50, 100, 200, and 500 mV s^{-1} were also investigated (see Supporting Information). The irreversible oxidation processes at low scan rates indicate

Table 4. Electrochemical Data and Energy Levels for **1**−**6**[a]

	E_a^{ox} V	E_{onset}^{ox} V	$E_{1/2}^{re}$ or E_c^{re} V	E_{onset}^{re} V	HOMO eV	LUMO eV	ΔE eV	ΔE[d] eV
1	0.96[b]	0.84	−1.75,[b] −2.08[b]	−1.65	−5.64	−3.15	2.49	2.85
2	0.95[b]	0.83	−1.68,[b] −2.07[b]	−1.60	−5.63	−3.20	2.43	2.84
3	0.97[b]	0.86	−1.51,[c] −1.99[b]	−1.42	−5.66	−3.38	2.28	2.69
4	0.96[b]	0.84	−1.38,[b] −1.99[b]	−1.23	−5.64	−3.57	2.07	2.58
5	0.92[b]	0.80	−1.36,[b] −1.98[b]	−1.20	−5.60	−3.60	2.00	2.53
6	0.98[b]	0.86	−0.99,[c] −2.06[b]	−0.90	−5.66	−3.90	1.76	2.47

[a] In acetonitrile (0.10 mol L^{-1} of Bu_4NPF_6) at 298 K, scan rate of 50 mV s^{-1}, all potentials versus SCE. [b] Irreversible wave. [c] Reversible wave. [d] Obtained from theoretical calculations.

that the oxidation products of all complexes are not stable. For complexes **3**, **4**, and **6**, the oxidation processes are all irreversible at any scan rates measured. But complexes **1**, **2**, and **5** showed improved reversibility at high scan rates, indicating the stability of oxidation products of **1**, **2**, and **5** was improved compared with that of **3**, **4**, and **6**. Meanwhile, compounds **1**−**6** exhibit the first and second reduction waves at ca. −0.99 to −1.75 and −1.98 to −2.08 V, respectively. The first reduction potential becomes less negative and the energy gap (ΔE) between the HOMO and LUMO become narrower from **1** to **6**. This is in accordance with the red-shift of emission wavelength from **1** to **6**. The first reduction potential can be assigned to the reduction of diimine ligands,[8] and the difference of the first reduction potential may be caused by the different conjugated length of diimine ligands. In addition, the similar second reduction potential for all complexes is assigned to the reduction of the C∧N ligand (piq), and this potential is also similar to the previous report.[18] The above discussions suggest that LUMOs are located on the diimine ligands. Hence, we can tentatively assign the excited states of the complexes to the mixed states of [dπ(Ir) → $\pi^*_{N\wedge N}$] MLCT transitions and [$\pi_{C\wedge N}$ → $\pi^*_{N\wedge N}$] LLCT transitions.

Theoretical Calculations. To further investigate the nature of the excited state, density functional theory (DFT) for **1**−**6** was performed. The distributions of molecular orbitals (HOMO−2, HOMO−1, HOMO, LUMO, LUMO+1, and LUMO+2) (see Table 5) and the calculated molecular orbital compositions of **1**−**6** (see ESI) are studied. All complexes have similar HOMO and LUMO distributions. The HOMO primarily resides on the iridium center and the phenyl groups of C∧N ligand (piq); the LUMO is mainly located on the N∧N ligands. Therefore, the excited states of the complexes can be assigned to a mixture of [dπ(Ir) → $\pi^*_{N\wedge N}$] MLCT transitions and [$\pi_{C\wedge N}$ → $\pi^*_{N\wedge N}$] LLCT transitions. This assignment has been verified by unresolved luminescence

(16) (a) Serroni, S.; Juris, A.; Campagna, S.; Venturi, M.; Denti, G.; Balzani, V. *J. Am. Chem. Soc.* **1994**, *116*, 9086−9091. (b) Calogero, G.; Giuffrida, G.; Serroni, S.; Ricevuto, V.; Campagna, S. *Inorg. Chem.* **1995**, *34*, 541−545. (c) Mamo, A.; Stefio, I.; Parisi, M. F.; Credi, A.; Venturi, M.; Di Pietro, C.; Campagna, S. *Inorg. Chem.* **1997**, *36*, 5947−5950. (d) Di Marco, G.; Lanza, M.; Mamo, A.; Stefio, I.; Di Pietro, C.; Romeo, G.; Campagna, S. *Anal. Chem.* **1998**, *70*, 5019−5023. (e) Didier, P.; Ortmans, I.; Kirsch-De Mesmaeker, A.; Watts, R. J. *Inorg. Chem.* **1993**, *32*, 5239−5245.

(17) Calogero, G.; Giuffrida, G.; Serroni, S.; Ricevuto, V.; Campagna, S. *Inorg. Chem.* **1995**, *34*, 541−545.

(18) Okada, S.; Okinaka, K.; Iwawaki, H.; Furugori, M.; Hashimoto, M.; Mukaide, T.; Kamatani, J.; Igawa, S.; Tsuboyama, A.; Takiguchi, T.; Ueno, K. *Dalton Trans.* **2005**, *9*, 1583−1590.

Table 5. HOMOs and LUMOs Distributions of **1**−**6**

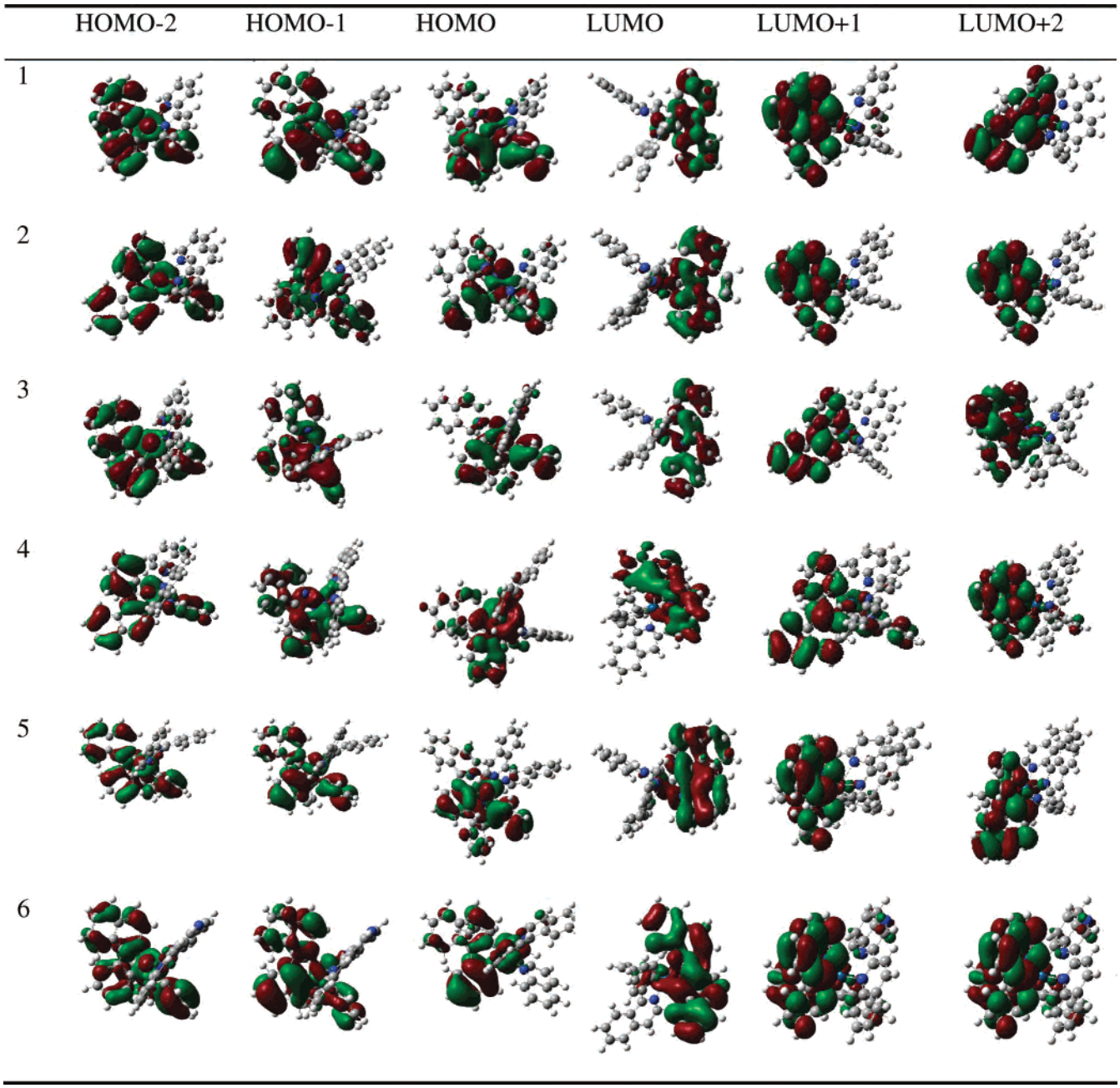

bands and the study of electrochemical properties. The calculated energy gaps (ΔE) between the HOMOs and LUMOs are listed in Table 4. Complexes **1** and **2** have similar energy gaps, and the energy gap (ΔE) of **3**−**6** decreased significantly, which is in agreement with the results deduced from electrochemical measurement and the phenomenon of red-shift of emission wavelength. Furthermore, this fact proves that the conjugated length of the diimine ligands is the key factor to the excited state properties of the complexes. The composition of the HOMO−1 is similar to that of HOMO. The LUMO+1 and LUMO+2 are mainly localized on the isoquinolyl groups of C∧N ligand (piq), and the phenyl groups of the C∧N ligand (piq) also have some LUMO+1 and LUMO+2 distribution. Compared with the HOMO−1 and HOMO, the composition of phenyl groups of C∧N ligand (piq) in the LUMO+1 and LUMO+2 decreases significantly. Instead, the composition of isoquinolyl groups of C∧N ligand (piq) in the LUMO+1 and LUMO+2 increases significantly. This may show that the HOMO (HOMO−1) → LUMO+1 (LUMO+2) transitions could contribute to the ^{3}LC($\pi_{C\wedge N} \rightarrow \pi^*_{C\wedge N}$) excited state.

Luminescence Spectroscopy. The room-temperature photoluminescence spectra in CH_2Cl_2 solution are shown in Figure 7 and the corresponding photophysical data of the iridium complexes are summarized in Table 6. The observed emission lifetimes in microsecond and sub-microsecond time scales indicate the phosphorescent nature of the emission. The emission wavelength from **1** to **6** can be tuned from 586 to 732 nm (see Figure 7). This is in agreement with the decrease of ΔE deduced by electrochemical data from **1** to

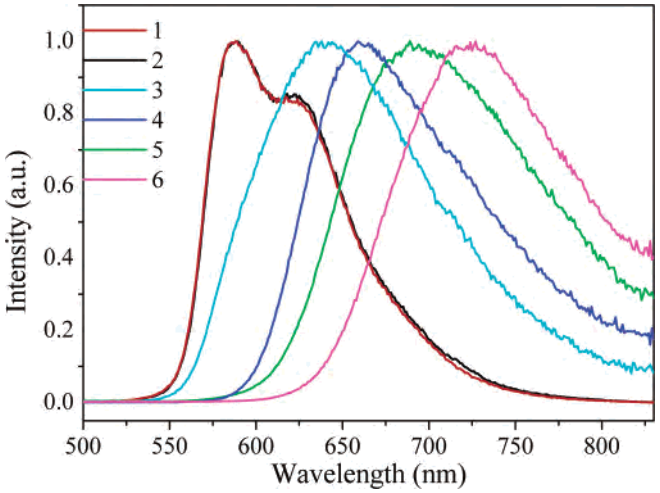

Figure 7. Room-temperature photoluminescence spectra of **1**−**6** in CH_2Cl_2.

Table 6. Photophysical Properties of **1**−**6**

	medium (T [K])	$\lambda_{PL,max}$ (nm)	Φ_{em}	τ (μs)
1	CH_2Cl_2 (298)	586	0.087	1.32
	CH_3CN (298)	588		
	glass (77)	580		4.12
2	CH_2Cl_2 (298)	589	0.083	0.86
	CH_3CN (298)	590		
	glass (77)	580		4.21
3	CH_2Cl_2 (298)	637	0.054	0.30
	CH_3CN (298)	643		
	glass (77)	590		4.42
4	CH_2Cl_2 (298)	659	0.018	0.49
	CH_3CN	678		
	glass (77)	612		5.95
5	CH_2Cl_2 (298)	695	0.005	0.11
	CH_3CN (298)	710		
	glass (77)	605		1.96
6	CH_2Cl_2 (298)	732	0.003	0.10
	CH_3CN (298)	760		
	glass (77)	656		4.13

6. Considering that all complexes have the same C∧N ligand, we can conclude that the decrease of ΔE and the red-shift of emission wavelength are caused by the change of the conjugated length of diimine ligands. The complex containing the ligand with longer conjugated length appears to have a more red-shifted luminescence. The attachment of extra aromatic rings into π framework of the diimine ligand from bpy to biqu could elongate the overall π conjugation and consequently decrease the energy levels of LUMOs. On the other hand, compared with ligand bqu, the replacement of one CH by an electronegative nitrogen atom in quqo would decrease the energy level of the diimine ligand furthermore. The effect of conjugated length on the energy levels of ligands can be seen by the variation of singlet energy levels of ligands, which can refer to the wavelengths of the UV−vis absorbance edges of the diimine ligands (see Supporting Information). The wavelengths of UV−vis absorbance edges of bpy, phen, pyqu, bqu, biqu, and quqo are 302, 303, 342, 347, 349, and 364 nm, respectively, indicating that their corresponding singlet energy levels are 33 113, 33 003, 29 240, 28 818, 28 653, and 27 472 cm^{-1}, respectively.

The low-temperature photoluminescence spectra of all complexes in ethanol−methanol (4:1, v:v) glass were studied and shown in Figure 8. For **1** and **2**, no evident blue-shift of

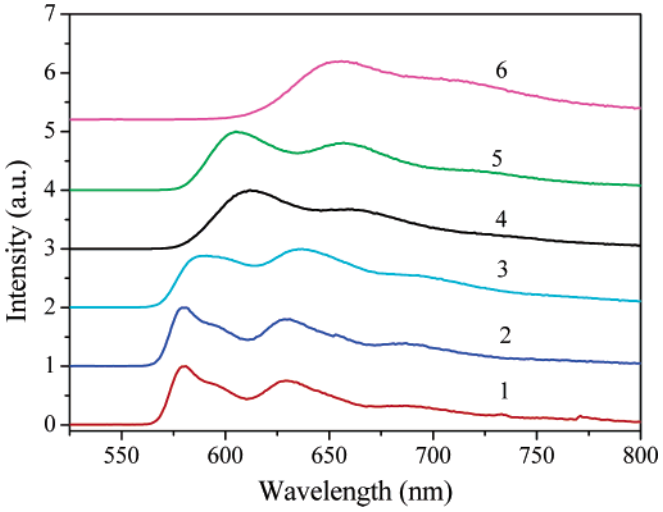

Figure 8. Photoluminescence spectra of **1**−**6** in EtOH/MeOH (4:1 v/v) at 77 K.

emission maxima from fluid solution at room temperature to rigid matrix at 77 K was observed (see Table 6). However, compared with the emission maxima at room temperature, an obvious blue-shift of the emission maxima of **3**−**6** at 77 K could be observed, which shows the excited-state properties of **3**−**6** are different from those of **1** and **2**. Furthermore, the photoluminescence spectra of all complexes in different solvents were also investigated and the data are summarized in Table 6. No obvious shift of photoluminescence spectra of **1** and **2** was observed by changing solvent, indicating that the photoluminescence spectra of **1** and **2** were evidently not dependent on the solvent polarity. However, the emission maxima occur at higher energy in less-polar CH_2Cl_2 than in more-polar CH_3CN for **3**−**6**.

For the small dependence on the solvent polarity and temperature of photoluminescence spectra for **1** and **2**, it can be concluded that the emission of **1** and **2** is caused by the special CT states mixed with more ligand-centered (cyclometalated) character (^{3}LC).[19] Güdel et al.[20] have observed the strong mixing between the LC ($\pi_{C\wedge N} \rightarrow \pi^*_{C\wedge N}$) and MLCT excited states in the similar cationic iridium complex $[Ir(ppy)_2bpy]^+$. The close proximity of the ^{3}LC and ^{3}MLCT excited states and the large strong spin−orbit coupling of Ir^{3+} induce the strong mixing of the charge-transfer and LC excited states.

Figure 7 shows that the photoluminescence spectra of **3**−**6** measured at 298 K are broad and structureless. According to the previous works,[1,8,18] the photoluminescence spectra from the ligand-centered $^3\pi-\pi^*$ state display vibronic progressions, while those from the CT state are broad and featureless. Therefore, we can conclude that charge-transfer state participates in the nature of such emissions for **3**−**6**. Moreover, according to previous report,[8] the sensitivity to the medium and temperature of photoluminescence spectra for **3**−**6** shows that the excited states for these complexes are mainly attributed to the CT states (including ^{3}MLCT and LLCT) and the contribution from ^{3}LC ($\pi_{C\wedge N} \rightarrow \pi^*_{C\wedge N}$) is relatively rare.

(19) Lo, K. K. W.; Ng, D. C. M.; Chung, C. K. *Organometallics* **2001**, *20*, 4999−5001.

Generally, for the cationic iridium(III) complexes containing diimine ligands, emission commonly comes from a mixed excited state containing ^{3}LC ($\pi_{C\wedge N} \rightarrow \pi^*_{C\wedge N}$) and ^{3}MLCT ($d\pi(Ir) \rightarrow \pi^*_{N\wedge N}$) transitions,[21,22] which can be described as follows.[12]

$$\Phi_T = a\Phi(^3LC) + b\Phi(^3MLCT) \quad (1)$$

where a and b are the normalized coefficients, $\Phi(^3LC)$ and $\Phi(^3MLCT)$ are the wave functions of ^{3}LC ($\pi_{C\wedge N} \rightarrow \pi^*_{C\wedge N}$) and ^{3}MLCT ($d\pi(Ir) \rightarrow \pi^*$ (diimine)) excited states, respectively. And the ^{3}LC state localized on the cyclometalated ligands (C$\wedge$N) have been proved by the previous reports.[23]

However, for the existence of LLCT transition in these iridium complexes, we consider the mixed excited states in the complex system should be described as follows.

$$\Phi_T = a\Phi(^3LC) + b\Phi(^3MLCT) + c\Phi(^3LLCT) \quad (2)$$

where c is the normalized coefficient and Φ (^{3}LLCT) is the wave function of ^{3}LLCT [$\pi_{C\wedge N} \rightarrow \pi^*_{N\wedge N}$] excited state.

From the above discussion, we can see that the normalized coefficients of $\Phi(^3LC)$, $\Phi(^3MLCT)$, and $\Phi(^3LLCT)$ are different for complexes **1**−**6**. For complexes **1**−**2**, the contribution of the excited state includes $^3LC(\pi_{C\wedge N} \rightarrow \pi^*_{C\wedge N})$, ^{3}MLCT ($d\pi(Ir) \rightarrow \pi^*$ (diimine)), and ^{3}LLCT [$\pi_{C\wedge N} \rightarrow \pi^*_{N\wedge N}$], whereas the excited states of the complexes **3**−**6** are mainly contributed to ^{3}MLCT ($d\pi(Ir) \rightarrow \pi^*_{N\wedge N}$) and ^{3}LLCT ($\pi_{C\wedge N} \rightarrow \pi^*_{N\wedge N}$) with little contribution of ^{3}LC ($\pi_{C\wedge N} \rightarrow \pi^*_{C\wedge N}$). As shown in Table 4, all complexes have similar energy levels of HOMO and different energy levels of LUMO, giving rise to different energies of the ^{3}MLCT ($d\pi(Ir) \rightarrow \pi^*$(diimine)). For the same cyclometalated ligand for these complexes, the energy of ^{3}LC ($\pi_{C\wedge N} \rightarrow \pi^*_{C\wedge N}$) for all complexes should be similar. Because of the less-conjugated length of the diimine ligands (bpy and phen), **1** and **2** have higher energy levels of ^{3}MLCT, which would increase the contributions from $^3LC(\pi_{C\wedge N} \rightarrow \pi^*_{C\wedge N})$. In contrast, with an increase of the conjugated length of the diimine ligands (pyqu, bqu, biqu, and quqo), complexes **3**−**6** have low-energy ^{3}MLCT, and the contributions from ^{3}LC ($\pi_{C\wedge N} \rightarrow \pi^*_{C\wedge N}$) are small. These facts indicate that the change of the diimine ligands greatly affects the photoluminescence properties of these complexes. In the previous reports, Williams[3c], Haga, [4d] and Lo[2c,2d] have observed the complicated excited states containing ^{3}MLCT, ^{3}LLCT, and 3LC excited states simultaneously in iridium(III) complexes. To the best of our knowledge, there are very few reports about the modulation of complicated excited states for iridium(III) complexes containing three kinds of excited states by changing the diimine ligands with different conjugated length.

Conclusions

In conclusion, we have demonstrated a series of new cationic iridium(III) complexes based on the diimine ligands with different conjugated lengths. The detailed study of the theoretical calculations and photophysical and electrochemical properties show that the excited state of complexes is complicated and contains triplet metal-to-ligand charge transfer (^{3}MLCT), triplet ligand-to-ligand charge transfer (^{3}LLCT), and ligand-centered (cyclometalated) (^{3}LC) transitions simultaneously. Importantly, the complicated excited state of iridium(III) complexes could be modulated by changing the conjugated length of the diimine ligands. Moreover, significant emission wavelength tuning (~150 nm) has been achieved by changing the conjugated length of the diimine ligands.

Acknowledgment. The authors thank the National Natural Science Foundation of China (20490210 and 20501006) and the Shanghai Science and Technology Community (05DJ14004) for financial support.

Supporting Information Available: Crystallographic information files for complexes **5**, **6**, and **2′**, absorption spectra of the N$\wedge$N ligands, the oxidation potentials of **1**−**6** at different scan rates, and the calculated molecular orbital compositions of **1**−**6**. This material is available free of charge via the Internet at http://pubs.acs.org.

IC052034J

(20) Colombo, M. G.; Hauser, A.; Gudel, H. U. *Inorg. Chem.* **1993**, *32*, 3088−3092.
(21) (a) Colombo, M. G.; Gudel, H. U. *Inorg. Chem.* **1993**, *32*, 3081−3087. (b) Wilde, A. P.; King, K. A.; Watts, R. J. *J. Phys. Chem.* **1991**, *95*, 629−634.
(22) Colombo, M. G.; Hauser, A.; Gudel, H. U. *Inorg. Chem.* **1993**, *32*, 3088−3092.
(23) (a) Colombo, M. G.; Zilian, A.; Gudel, H. U. *J. Am. Chem. Soc.* **1990**, *112*, 4581−4582. (b) Colombo, M. G.; Zilian, A.; Gudel, H. U. *J. Lumin.* **1991**, *49*, 549−552. (c) Zilian, A.; Giidel, H. U. *Inorg. Chem.* **1992**, *31*, 830−835. (d) Zilian, A.; Gudel, H. U. *J. Lumin.* **1992**, *51*, 237−247.